CONSTRAINING LENS MODELS USING DOUBLE QUASARS PREDICTED FOR THE ROMAN SPACE TELESCOPE

LINDITA HAMOLLI[1], ESMERALDA GULIQANI[2], MIMOZA HAFIZI[1]

[1]Department of Physics, Faculty of Natural Sciences, University of Tirana, Albania

[2]Department of Mathematics and Physics, Faculty of Natural and Human Sciences, "Fan S. Noli" University of Korça, Albania

e-mail: lindita.hamolli@fshn.edu.al

Abstract

Constraining the mass distribution of lensing galaxies in strongly lensed quasars is a fundamental challenge in gravitational lensing, as it directly affects the interpretation of key astrophysical and cosmological parameters. In this study, we assess the capability of the Roman Space Telescope (Roman) to distinguish between spherical and elliptical lens models in the case of double quasars. Using Monte Carlo simulations, we generate a synthetic population of quasar–galaxy lensing systems, incorporating their observed redshift distributions and the galaxy stellar mass function. Modeling the lensing galaxy as a Singular Isothermal Ellipsoid (SIE), we compute the positions of the lensed images by solving the lens equation. The simulation results confirm that double-image configurations dominate, representing over 80% of all strong lensing events. We adopt Roman's expected angular resolution of 0.1 arcseconds as the detection threshold for image separation. Based on this criterion, we evaluate the geometric alignment of images with the lensing galaxy in double lensed quasars to determine whether the lens mass distribution can be reliably classified as spherical or elliptical. We find that in approximately 30% of double-image cases, the image configuration deviates sufficiently from perfect alignment to allow meaningful constraints on lens ellipticity. These results highlight both the potential and the observational limitations of the Roman Telescope in probing the internal structure of lensing galaxies.

Key words**:** *quasar, galaxy, strong lensing.*

Përmbledhje

Kufizimi i shpërndarjes së masës në galaktikat lente të kuazarë të lensuar përbën një sfidë themelore në lensimin gravitacional, pasi ndikon drejtpërdrejt në interpretimin e parametrave kyç në astrofizikë dhe kozmologji. Në këtë studim, ne vlerësojmë aftësinë e teleskopit hapësinor Roman për të dalluar midis modeleve sferike dhe eliptike të shpërndarjes së masës të lenteve në rastin e kuazarëve me dy imazhe. Duke përdorur simulime Monte Carlo, gjenerojmë një popullim sintetik të sistemeve kuazar–galaktikë, duke përfshirë shpërndarjet e redshifteve të tyre dhe funksionin e masës yjore të galaktikave. Duke modeluar galaktikën lente si një Elipsoid Izotermal Singular (SIE), ne kalkulojmë pozicionet e imazheve nga zgjidhja e ekuacionin të lentes. Rezultatet e simulimit konfirmojnë se konfigurimet me dy imazhe dominojnë, duke përfaqësuar mbi 80% të të gjitha rasteve. Ne marrim si prag dedektimi të kuazareve të lensuar rezolucionin këndor prej 0.1 arcsekondash, të parashikuar për teleskopin Roman. Bazuar në këtë kriter, ne vlerësojmë rreshtimin gjeometrik të dy imazheve me qendrën e galaktikës për të përcaktuar nëse shpërndarja e masës së lentes mund të klasifikohet si sferike apo eliptike. Gjejmë se në rreth 30% të kuazarëve me dy imazhe, konfigurimi i imazheve devijon mjaftueshëm nga rreshtimi perfekt për të mundësuar kufizime mbi elipticitetin e lentes. Këto rezultate hedhin dritë si mbi potencialin ashtu edhe limitet vrojtuese të teleskopit Roman në studimin e strukturës së brendshme të galaktikave që veprojnë si lente gravitacionale.

Fjalë kyçe: *kuazar, galaksi, lensimi i fortë.*

Introduction

Quasars are among the most luminous and energetic objects in the distant universe. The MILLIQUAS catalog (Flesch, 2019), which compiles data from a wide range of astronomical surveys up to December 2019, lists over 1,021,800 confirmed quasars, with redshifts reaching up to 8. When a massive galaxy is positioned along the line of sight between a quasar and the observer, the gravitational field of the intervening galaxy can bend the quasar's light and produce multiple images of the same source, a phenomenon known as strong gravitational lensing. These lensed images are typically separated by a few arcseconds. So far, approximately 220 lensed quasars[1] have been identified, the majority of which are two-image (double) systems. In more than 90% of these cases, the image separation exceeds 1 arcsecond, a scale that strongly

[1] https://research.ast.cam.ac.uk/lensedquasars/

depends on the angular resolution of the observational instrument (Hamolli et al., 2024). Systems with smaller separations may remain undetected by current telescopes but are expected to be revealed by upcoming missions, such as the Roman Space Telescope (Spergel et al., 2015; Hamolli et al., 2023a).

Depending on the relative alignment between the quasar and the intervening galaxy, as well as the mass distribution model of the lens, the light from a distant quasar may be bent to produce two, three, or even four separate images. Such phenomena are highly valuable in astrophysics and cosmology, as they provide insight into several fundamental aspects: the total projected mass enclosed within the Einstein radius, which includes both visible and dark matter; the gradient of the inner mass density profile of the lensing galaxy; the internal structure of the quasar; and constraints on cosmological parameters, with particular emphasis on the Hubble constant H_0 (Wong et al., 2020).

One of the main challenges in the analysis of strong gravitational lensing events is the precise modeling of the mass distribution within the lensing galaxy. The most commonly used model is the Singular Isothermal Sphere (SIS), which assumes spherical symmetry, but more complex models such as the Nonsingular Isothermal Sphere (NIS) (see Hamolli et al., 2023b) and the Singular Isothermal Ellipsoid (SIE) (Kormann et al., 1994) are also considered. In the SIS and NIS models, double or triple quasar images lie along the same straight line that connects the source (quasar) with the center of the lensing galaxy. In contrast, the SIE model, which accounts for elliptical mass distributions, can produce up to four images that are generally not collinear. Consequently, a double quasar configuration can arise from either a spherical or an elliptical lens. In the case of a spherical lens, the images are perfectly aligned with the galaxy center; however, this alignment is typically broken when the lens has ellipticity. The more elliptical the lens, the greater the deviation of the images from perfect alignment. Analyzing such configurations provides insight into the lens's sphericity. In this paper, we focus on evaluating the capability of the Roman Space Telescope to constrain lens models in double quasar systems expected to be detected in its surveys.

The Roman Space Telescope is an infrared observatory developed by NASA, scheduled for launch in May 2027, and will operate at the second Lagrange point (L2). Its primary scientific objective is to investigate dark energy using a combination of observational techniques. The telescope is equipped with the

Wide Field Instrument (WFI)[2], which includes eight filters spanning wavelengths from 0.48 to 2.3 μm, along with a coronagraph designed for high-contrast imaging. The WFI provides a field of view of 0.281 square degrees and, over the course of a five-year mission, is expected to survey approximately 2,000 square degrees through near-infrared imaging and spectroscopy, achieving an angular resolution of 0.1 arcseconds (Spergel et al., 2015).

The structure of this paper is as follows: Section II provides a brief overview of gravitationally lensed quasars by spherical and elliptical galaxies. Section III describes the simulation methodology and presents the results. The paper concludes with our main findings and discussing their overall impact.

Strong lensing of quasars

In lensed quasars, light emitted by a background source travels across vast cosmic distances before reaching the observer. Given that the physical thickness of the lensing galaxy is negligible compared to these distances, the system can be accurately described using the "thin lens" approximation (Schneider et al., 1992). Within this framework, the mass of the lens is projected onto a two-dimensional plane perpendicular to the observer's line of sight. Let $\vec{\beta}$ denote the true angular position of the source, $\vec{\theta}$ the observed angular position of the image, and $\vec{\alpha}(\vec{\theta})$ the scaled deflection angle. The lens equation can then be expressed as (Meylan et al., 2006),

$$\vec{\beta} = \vec{\theta} - \vec{\alpha}(\vec{\theta}). \tag{1}$$

The scaled deflection angle $\vec{\alpha}(\vec{\theta})$ is related to the physical deflection angle $\vec{\hat{\alpha}}(\vec{\theta})$, through the relation $\vec{\alpha}(\vec{\theta}) = \frac{D_{LS}}{D_S}\vec{\hat{\alpha}}(\vec{\theta})$, where D_{LS}, D_S are the angular diameter distances from the lens to the source and from the observer to the source, respectively. The lens equation is generally non-linear, meaning that for a given source position $\vec{\beta}$, there may be multiple solutions for $\vec{\theta}$, corresponding to multiple images of the source.

The magnification of each image depends on the specific alignment between the source and the lens. When the magnification formally diverges, the corresponding source positions define a curve in the source plane known as the *caustic*, and the associated image positions lie along the *critical curve* in

[2] Wide Field Instrument - Technical - Roman Space Telescope/NASA

the image plane. These curves typically form closed shapes, and the number of images changes by two whenever the source crosses a caustic.

In realistic cases, sources have a finite size and thus do not experience infinite magnification. Instead, the amplification is averaged over the surface of the source. In addition to caustics, lensing systems can also exhibit *cut curves*, which separate regions in the source plane where one or more images become effectively undetectable, either due to extreme demagnification or because an image lies too close to the lens center to be resolved. Unlike caustics, cut curves do not correspond to singularities in magnification, but they still mark changes in the number of observable images. For this reason, they are often called *pseudo-caustics* and play an important role in determining the actual image configurations observed (Meneghetti, 2021).

Spherical lensing mass distribution

The simplest model used to describe the mass distribution in strongly lensing galaxies is the Singular Isothermal Sphere (SIS). In this model, the mass density is given by $\rho(r) = {\sigma_{SIS}}^2/2\pi G r^2$, where σ_{SIS}, is the one-dimensional velocity dispersion of stars in the galaxy, and r is the radial distance from the galactic center (Eigenbrod, 2011). Despite representing a central singularity and implying an infinite total mass, the SIS model remains a useful approximation for understanding the basic properties of gravitational lensing. The mass enclosed within an angular radius θ is expressed as: $M(\theta) = \frac{\pi {\sigma_{SIS}}^2}{G}\theta D_L$ while the corresponding Einstein angular radius is: $\theta_0 = \frac{4\pi {\sigma_{SIS}}^2}{c^2}\frac{D_{LS}}{D_S}$. When the source lies inside the Einstein ring (i.e., $\beta < \theta_0$), the lens equation has two solutions: $\theta_A = \beta + \theta_0$ and $\theta_B = \beta - \theta_0$. These two images appear on opposite sides of the lensing galaxy, one inside and one outside the Einstein ring, separated by an angular distance $\Delta\theta = 2\theta_0$ (see Hamolli et al., 2023b for more details). The critical curve in the image plane corresponds to a circle of radius θ_0, where the magnification formally diverges. Its mapping under the lens equation in the source plane corresponds to a single point at the origin, known as the caustic. The SIS model also predicts a *cut curve* at $\beta = \theta_0$, in the source plane, beyond which one of the theoretical images becomes practically undetectable. This occurs because the inner image lies extremely close to the lens center and is severely demagnified.

To address the unrealistic central singularity in the SIS model, the Non-Singular Isothermal Sphere (NIS) model introduces a finite-density core. Its mass density is given by: $\rho(r) = \frac{{\sigma_{SIS}}^2}{2\pi G}\left(\frac{1}{r^2+r_c^2}\right)$, where $r_c = \theta_c D_L$ is the physical core radius. The Einstein angular radius in the NIS model is modified to: $\theta_{ENIS} = \theta_0\sqrt{1-\frac{2\theta_C}{\theta_0}}$. If the core radius, θ_c, is smaller than half the Einstein radius θ_0, the lens equation can yield either one or three images, depending on the source's position. This model introduces two critical curves in the image plane: a tangential critical curve near the Einstein radius and a radial critical curve closer to the lens center. These correspond to two distinct caustics in the source plane: the tangential caustic, which reduces to a single point at the origin, and the radial caustic, which typically forms a closed curve surrounding it. When the source lies within the radial caustic, three images aligned along the line passing through the galactic center are produced. However, in most cases, only two are detectable, as the central image is highly demagnified and located very close to the lens center. The size of the lens core thus plays a key role in determining the number, positions, and detectability of the resulting images (Mollerach & Roulet, 2002). In these models, the lensed images are collinear with the galaxy center, forming along the same line.

Elliptical lens mass distribution

A more realistic alternative to the lens models commonly used in strong gravitational lensing is the Singular Isothermal Ellipsoid (SIE). This model describes a lens whose projected mass distribution takes an elliptical form, breaking spherical symmetry through a flattening parameter defined as the axis ratio $f = b/a$, where a and b are the major and minor axes of the projected ellipse, respectively. The surface mass density is given by:

$$\Sigma(\xi) = \frac{\sigma^2}{2G}\frac{\sqrt{f}}{\sqrt{\xi_1^2+f^2\xi_2^2}}, \tag{2}$$

where ξ_1 and ξ_2 are coordinates in the lens plane (Kormann et al., 1994).

Unlike the spherical models, the SIE model introduces anisotropy in the lens potential, as the deflection angle depends on the angular position of the light ray. This added complexity leads to a wider range of image configurations, including two, three, or four images, depending on the source's location relative to the caustics and cut curves in the source plane.

Unlike the SIS model, which produces a circular critical curve (Einstein ring), the SIE model produces a tangential critical curve that is elongated along the major axis of the lens. Its mapping into the source plane forms an astroid-shaped caustic, which is a diamond-like curve centered on the optical axis. When the source lies outside this caustic, two lensed images are typically formed.

If the source is located inside the caustic, four images may result, arranged asymmetrically depending on the source's exact position. For this model, the cut curve is typically elongated along the minor axis and does not coincide with the caustic. It plays a critical role in determining which regions of the source plane produce a specific number of observable images.

A key parameter influencing the number of visible images is the axis ratio f. When $f > 0.3942$ the lens system can produce up to four distinct images, depending on the source's position relative to the caustic and cut curves. As the source moves inward, all four images may become visible, forming a symmetric Einstein Cross. In contrast, when $f \leq 0.3942$ a three-image configuration becomes possible due to the cut curve shifting closer to the caustic, allowing the central image to remain detectable (Meneghetti, 2021).

Figure 1 presents the lensing configurations for cases one, two, three, or four images. In all panels, the source lies in the first quadrant, while the axis ratio *f* and position angle (*PA*) of the lens vary. The number and spatial distribution of lensed images are affected by the source's position relative to the caustic and cut curves, as well as by the shape and orientation of the lensing mass distribution. Since our interest lies in quasars producing two lensed images within this model, it should be emphasized that these images are never collinear with the galactic center

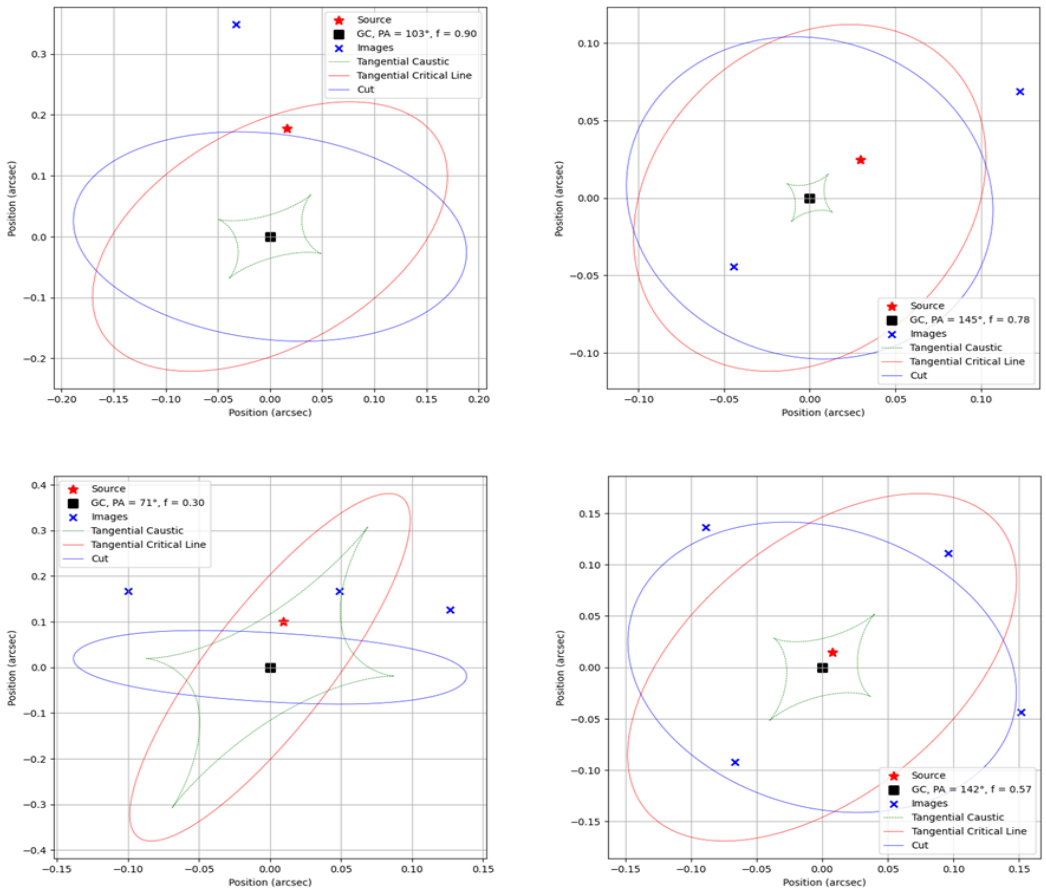

Figure 1. Configurations of a lensed quasar system producing one, two, three, and four images. The black square marks the center of the lensing galaxy, while the red star represents the position of the background quasar (source), which in all panels lies in the first quadrant of the source plane. The blue crosses denote the lensed images. The red ellipse shows the tangential critical curve, the green dashed curve is the tangential caustic, and the blue solid curve represents the cut line. Each panel corresponds to a different combination of the lens axis ratio f and position angle PA, as indicated in the legends

Simulations and Results

To assess the capability of the Roman Space Telescope in constraining lens models for doubly lensed quasars, we employed a Monte Carlo approach. The

simulations were designed to generate galaxy–quasar pair parameters based on observed redshift distributions of quasars and galaxies, the stellar mass of lensing galaxies, and the empirical relation between stellar mass and velocity distributions. Specifically, we generated:

-*the quasar redshift* using data from the MILLIQUAS (Millions of Quasars) catalog[3] (Flesch, 2019), which contains 1,021,800 observed quasars. We have shown their distribution in Figure 2.

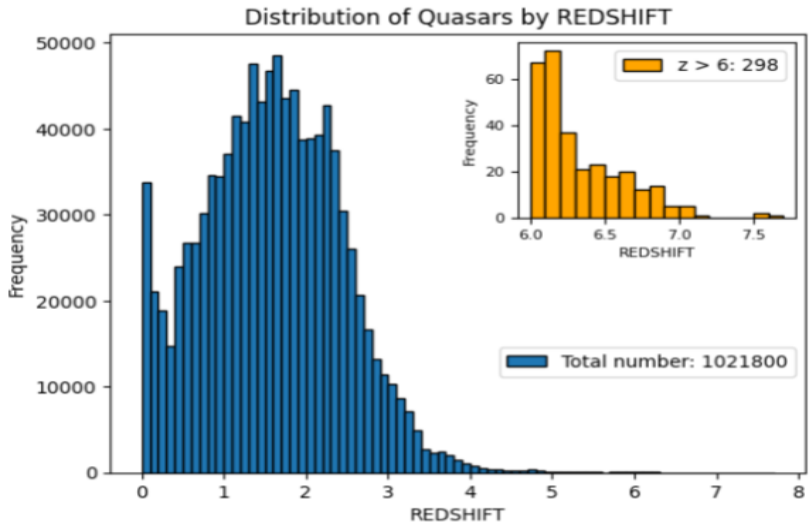

Figure 2. Histogram of quasars from the MILLIQUAS catalog as a function of redshift. Blue bars show the distribution of 1,021,800 quasars, while the inset highlights those with z > 6 in orange. Bin width = 0.1**.**

-*the galaxy redshift*, using the distribution obtained by Appenzeller et al. (2004), with the restriction that the galaxy redshift must be smaller than that of the corresponding quasar. For each quasar, the total number of galaxies satisfying this condition was determined from the cumulative galaxy distribution

-*the galaxy stellar mass* by relation obtained from Davidzon et al. (2017). Using the COSMOS2015 catalog, the authors provided a comprehensive view of the stellar mass assembly of galaxies across the redshift range $z = 0.1$ to

[3] https://heasarc.gsfc.nasa.gov/W3Browse/all/milliquas.html

$z = 6$. The measurements were fitted with a double Schechter function up to $z = 3$, and with a single Schechter function beyond that limit. The Schechter function is expressed as:

$$\phi(M)\, dM = \left[\phi_1^* \left(\frac{M}{M_*}\right)^{\alpha_1} + \phi_2^* \left(\frac{M}{M_*}\right)^{\alpha_2}\right] \exp\left(-\frac{M}{\mathrm{M}_*}\right) \frac{dM}{\mathrm{M}_*} \tag{3}$$

where the parameters of the COSMOS2015 stellar mass function (SMF), including M_*, α_1, ϕ_1^*, α_2, and ϕ_2^*, are reported in Table 1 of Davidzon et al. (2017).

-the stellar velocity dispersion was derived from the relation proposed by Zahid et al. (2016). By analyzing data from the SDSS and SHELS surveys, the authors established a correlation between the central stellar velocity dispersion and the stellar mass of galaxies, expressed as,

$$\begin{cases} \sigma(M) = \sigma_b \left(\frac{M}{M_b}\right)^{\alpha_1} \text{ for } M \le M_b \\ \sigma(M) = \sigma_b \left(\frac{M}{M_b}\right)^{\alpha_2} \text{ for } M > M_b \end{cases} \tag{4}$$

The best-fit parameters are $\log(M_b/M_\odot) = 10.26$, $\log(\sigma_b) = 2.073$, $\alpha_1 = 0.40$, and $\alpha_2 = 0.293$. The two indices $\alpha_1$and α_2 define the slopes of the power-law relation below and above the break point, respectively.

Assuming a flat universe with cosmological parameters: $\Omega_m = 0.30$, $\Omega_k = 0$, $\Omega_\Lambda = 0.70$, and $H_0 = 70$ km s^{-1}Mpc^{-1}, we calculated the angular diameter distances from the redshifts following Liao (2019),

$$D_L = \frac{c}{H_0(1+z_L)} \int_0^{z_L} \frac{dz}{E(z)},\ D_S = \frac{c}{H_0(1+z_S)} \int_0^{z_S} \frac{dz}{E(z)},\ D_{LS} = D_S - \frac{1+z_L}{1+z_S} D_L,$$

ku, $E(z) = \sqrt{\Omega_m (1+z)^3 + \Omega_k (1+z)^2 + \Omega_\lambda}$. (5)

For each quasar–galaxy pair, we computed the Einstein angle by $\theta_0 = \frac{4\pi\sigma^2}{c^2}\frac{D_{LS}}{D_S}$, since the measured central stellar velocity dispersion of the lens galaxy reflects the total mass enclosed within the Einstein radius, and provides a velocity scale consistent with that derived from the singular isothermal sphere model (Bolton et al., 2008). The probability that a galaxy lies within the Einstein angle along the quasar–galaxy line of sight is given by $10^8\, \theta_0^2/14$, normalized to the total number of galaxies, estimated at 200 billion across the sky (Beckwith et al., 2006). Each system was accepted as a

lensing event if a uniformly drawn random number in the interval (0, 1) was smaller than the estimated lensing probability; otherwise, it was rejected. This procedure was applied to the entire quasar sample.

We simulated a population of 100,000 strong lensing events. By applying an angular resolution limit of 0.1 arcseconds, corresponding to the expected performance of the Roman Space Telescope, we identified 578 quasars lensed by a single galaxy, with Einstein angular radius above the detection threshold. For each lensing galaxy, we employ a SIE model, and since for this model we needed the axis ratio f and position angle (PA) we extracted them from the HyperLeda catalog[4], where the position angle defines the orientation of the galaxy's major axis measured from North ($PA = 0$ corresponds to a North–South alignment).

For each of these systems, we computed the image positions, which may consist of one, two, three, or four distinct images depending on the geometry of the system, the axis ratio, and the orientation angle. Figure 3 presents configurations of lensed images for different multiplicity cases, along with the probability associated with each configuration. The results indicate that systems with two images dominate, comprising approximately 83% of all lensing events. Single-image systems occur in about 9% of cases, while configurations with three or four images are much less frequent, with probabilities of 2% and 7%, respectively.

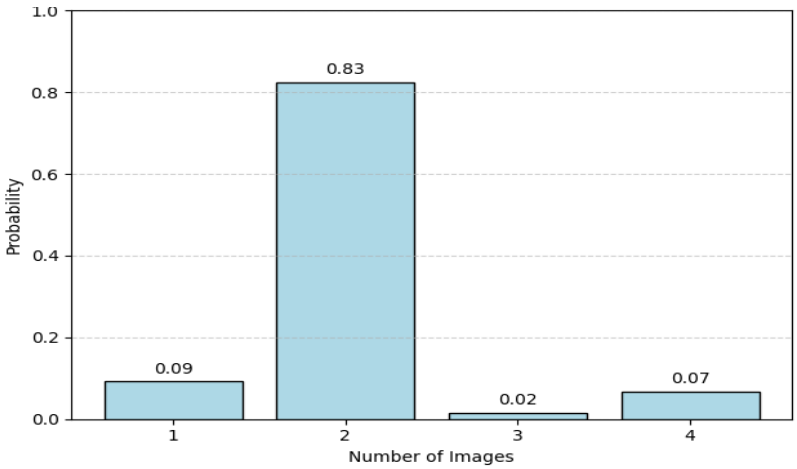

[4] http://atlas.obs-hp.fr/hyperleda/a106/

Figure 3. Probability distribution of the number of lensed images in the simulated quasar sample. Double-image systems dominate the population, accounting for 83% of cases. Single-image configurations occur in 9% of events, while three- and four-image systems are less frequent, with probabilities of 2% and 7%, respectively.

We focus on double-image systems, which may arise from either spherical or elliptical mass distributions of the lensing galaxy. When the angular separation of one image from the line connecting the other image and the galaxy center is smaller than the instrument's angular resolution, the system can effectively be interpreted as originating from a spherical mass distribution, even if the true lens is elliptical. We therefore investigate the capability of the Roman Space Telescope to constrain the lens mass distribution through observations of doubly imaged quasars.

For the double quasars in our sample, we calculated for each system the perpendicular distance of the second image from the line connecting the first image and the galaxy center. Figure 4 illustrates such a configuration: the magenta dashed line connects the galaxy center to the first image (shown in green), while the cyan dashed line extends perpendicularly from the second image (in blue), indicating its angular deviation from perfect alignment. The overall distribution of these distances across all simulated events is shown in Figure 5.

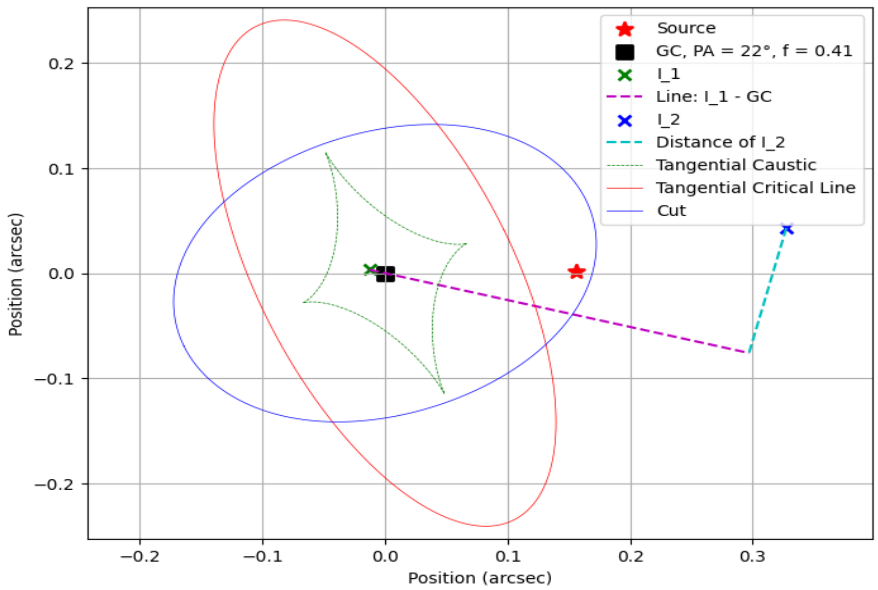

Figure 4. Configuration of a doubly lensed quasar. The black square marks the center of the lensing galaxy, the red star indicates the source position, and the two lensed images are shown in green and in blue color. The cut curve (solid blue line), the caustic (dashed green line), and the critical curve (solid red line) are included. This configuration corresponds to an axis ratio f = 0.41, and position angle PA=22°. The magenta dashed line connects the first image to the center of the lensing galaxy, while the cyan dashed line, drawn perpendicular to it, indicates the angular offset of the second image.

In this figure, the bin width is 0.1 arcseconds, is chosen to match the angular resolution of the Roman Space Telescope. For most double-quasar systems the measured distance falls within the first bin, accounting for roughly 70% of the cases. Consequently, such systems would be effectively interpreted as arising from a spherical mass distribution, even if the actual lens is elliptical, and the Roman telescope can reliably distinguish the lens mass distribution in only about 30% of events.

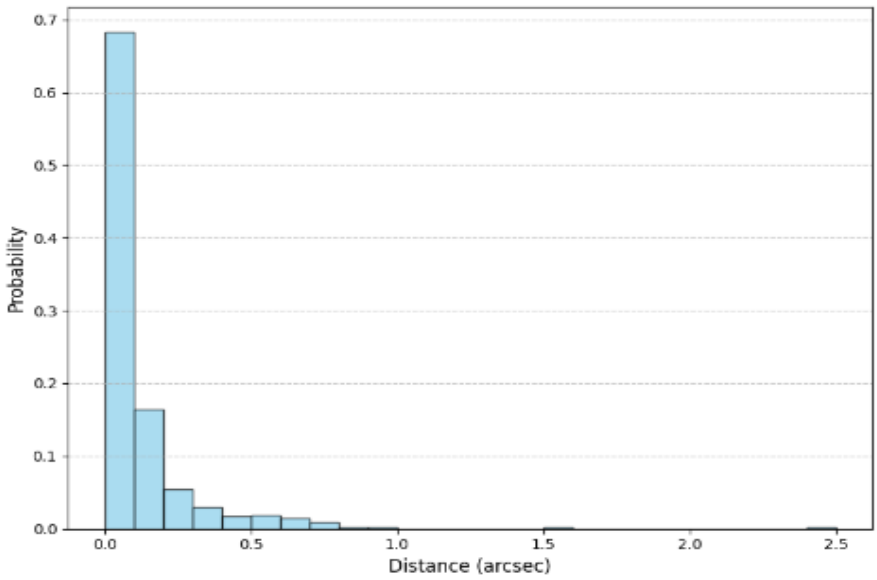

Figure 5. Probability distribution of the angular distances of the second image from the line connecting the first image and the center of the lensing galaxy. The values range from 0 to 2.5 arcseconds, with a bin width of 0.1 arcseconds.

Conclusions

In this study, we extended our previous work to evaluate the potential of the Roman Space Telescope to constrain the mass distribution of lensing galaxies using doubly lensed quasars expected to be detected by the mission. We assumed that a strong lensing event is observable if the separation between the lensed images—typically on the order of the Einstein radius—exceeds the telescope's angular resolution.

We simulated a synthetic population of 100,000 galaxy–quasar systems and adopted a detection threshold of 0.1 arcseconds, corresponding to Roman's expected resolution. For each system, considering a SIE mass distribution, we computed the image positions, which may result in one, two, three, or four distinct configurations. In the case of double quasars, we further calculated the angular displacement of one image relative to the line connecting the other image with the center of the lensing galaxy. Our results show that

approximately 70% of the simulated double quasars exhibit an angular deviation smaller than 0.1 arcseconds. Consequently, in about 70% of the double quasars expected to be observed by Roman, the lens galaxy would be interpreted as having a spherical mass distribution, while the remaining 30% are expected to reveal signatures more consistent with elliptical mass profiles.

Constraining the lens mass distribution is essential in strong lensing studies, as it directly influences time-delay measurements, which are key to determining cosmological parameters such as the Hubble constant (H□). Given the ongoing tension surrounding H□ and the potential of lensed quasars to provide an independent estimate, accurately modeling the lens mass distribution becomes critically important.

References

Appenzeller, I., Bender, R., Böhm, A., Stephan, F., Fricke, K. J., Gabasch, A., Heidt, J., Hopp, U., Jäger, K., Mehlert, D., Noll, S., Saglia, R., Seitz, S., Tapken, C., & Ziegler, B. (2004). Exploring Cosmic Evolution with the FORS Deep Field. The Messenger, 116, 18–24. http://pubman.mpdl.mpg.de/pubman/item/escidoc:949258

Beckwith, S., Stiavelli, M., Koekemoer, A. M., Caldwell, J. A. R., Ferguson, H. C., Hook, R. N., Lucas, R. A., Bergeron, L., Corbin, M. R., Jogee, S., Panagia, N., Robberto, M., Royle, P., Somerville, R. S., & Sosey, M. (2006). The Hubble Ultra Deep field. The Astronomical Journal, 132(5), 1729–1755. https://doi.org/10.1086/507302

Bolton, A. S., Treu, T., Koopmans, L. V. E., Gavazzi, R., Moustakas, L. A., Burles, S., Schlegel, D. J., & Wayth, R. (2008). The Sloan Lens ACS Survey. VII. Elliptical galaxy scaling laws from direct observational mass measurements. *The Astrophysical Journal*, 684(2), 248–259. https://doi.org/10.1086/589989

Davidzon, I., Ilbert, O., Laigle, C., Coupon, J., McCracken, H. J., Delvecchio, I., Masters, D., Capak, P., Hsieh, B. C., Le Fèvre, O., Tresse, L., Bethermin, M., Chang, Y. -Y., Faisst, A. L., Le Floc'h, E., Steinhardt, C., Toft, S., Aussel, H., Dubois, C., Hasinger, G., Salvato, M., Sanders, D. B., Scoville, N., Silverman, J. D. (2017). The COSMOS2015 galaxy stellar mass function. Thirteen billion years of stellar mass assembly in ten snapshots. Astron. Astrophys, 605, A70.

https://doi.org/10.1051/0004-6361/201730419

Eigenbrod, A., (2011). Gravitational lensing of quasars. CRC Pres.

Flesch, E. W. (2019). The Million Quasars (Milliquas) Catalogue, v6.4. Astrophysics of Galaxies. 1-6.

https://doi.org/10.48550/arXiv.1912.05614.

Hamolli, L., Hafizi, M., De Paolis, F., Guliqani, E. (2023a). Investigating Gravitationally Lensed Quasars Observable by Nancy Grace Roman Telescope. Galaxies, 11(3), 71. https://doi.org/10.3390/galaxies11030071

Hamolli, L., Guliqani, E., Hafizi, M. (2023b). The influence of the lens model on time delay during strong lensing by galaxies. Journal of Natural Science, 33, 3-20. https://jns.edu.al/publication-no-33-year-2023

Hamolli, L., Guliqani, E., Hafizi, M. (2024). Multiple Delays In Light Curves Of Lensed Quasars. Journal of Natural Science, 35, 184-196.

https://jns.edu.al/publication-no-35-year-2024/

Kormann, R., Schneider, P., Bartelmann, M. (1994). Isothermal elliptical gravitational lens models. Astronomy and Astrophysics, 284, 285-299.

http://adsabs.harvard.edu/abs/1994A%26A...284..285K

Liao, K. (2019). Measuring the Distances to Quasars at High Redshifts with Strong Lensing. The Astrophysical Journal, 883(1), 3.

https://doi.org/10.3847/1538-4357/ab39e6

Meneghetti, M. (2021). Introduction to Gravitational Lensing With Python Examples, Lecture notes in Physics, Springer, 956.

https://doi.org/10.1007/978-3-030-73582-1

Meylan, G., Jetzer, P., North, P., Schneider, P., Kochanek, C. S., & Wambsganß, J. (2006). Gravitational lensing: strong, weak and micro. In Saas-Fee Advanced Course. https://doi.org/10.1007/978-3-540-30310-7

Mollerach, S., & Roulet, E. (2002). Gravitational lensing and microlensing. World Scientific.

Schneider, P., Ehlers, J., & Falco, E. (1992). Gravitational lenses. In Astronomy and astrophysics library.

https://doi.org/10.1007/978-3-662-03758-4

Spergel, D. N., Gehrels, N., Baltay, C., Bennett, D. P., Breckinridge, J. B., Donahue, M., Dressler, A., Gaudi, B. S., Greene, T. P., Guyon, O., Hirata, C., Kalirai, J., Kasdin, N. J., Macintosh, B., Moos, W., Perlmutter, S., Postman, M., Rauscher, B. J., Rhodes, J., Zhao, F. (2015). Wide-Field InfrarRed Survey Telescope-Astrophysics Focused Telescope Assets WFIRST-AFTA 2015 Report. arXiv (Cornell University).

http://arxiv.org/pdf/1305.5422.pdf

Wong, K., Suyu, S., Chen, G., Rusu, C., Millon, M., Sluse, D., Bonvin, V., Fassnacht, C., Taubenberger, S., Auger, M., et al. (2020). H0LiCOW–XIII. A 2.4 per cent measurement of H0 from lensed quasars: 5.3 σ tension between early-and late-Universe probes. Monthly Notices of the Royal Astronomical Society, 498(1), 1420-1439.

https://doi.org/10.1093/mnras/stz3094

Zahid, H. J., Geller, M. J., Fabricant, D. G., & Hwang, H. S. (2016). The scaling of stellar mass and central stellar velocity dispersion for quiescent galaxies atz< 0.7. The Astrophysical Journal, 832(2), 203.

https://doi.org/10.3847/0004-637x/832/2/203